nature physics

LETTERS

PUBLISHED ONLINE: 4 DECEMBER 2011 | DOI: 10.1038/NPHYS2154

# Approaching zero-temperature metallic states in mesoscopic superconductor–normal–superconductor arrays

Serena Eley[1], Sarang Gopalakrishnan[1], Paul M. Goldbart[2] and Nadya Mason[1]*

**Systems of superconducting islands placed on normal metal films offer tunable realizations of two-dimensional (2D) superconductivity[1,2]; they can thus elucidate open questions regarding the nature of 2D superconductors and competing states. In particular, island systems have been predicted to exhibit zero-temperature metallic states[3–5]. Although evidence exists for such metallic states in some 2D systems[6,7], their character is not well understood: the conventional theory of metals cannot explain them[8], and their properties are difficult to tune[7,9]. Here, we characterize the superconducting transitions in mesoscopic island-array systems as a function of island thickness and spacing. We observe two transitions in the progression to superconductivity. Both transition temperatures exhibit unexpectedly strong depression for widely spaced islands, consistent with the system approaching zero-temperature ($T = 0$) metallic states. In particular, the first transition temperature seems to linearly approach $T = 0$ for finite island spacing. The nature of the transitions is explained using a phenomenological model involving the stabilization of superconductivity on each island via a coupling to its neighbours.**

Conventional zero-temperature ($T = 0$) metallic states do not exist in 2D systems possessing any disorder, because of Anderson localization[8,9]. To reconcile this fact with experimental evidence for $T = 0$ metals in 2D, it has been proposed that the experimental observations do not pertain to conventional metals, but rather to spatially inhomogeneous superconducting (or, more generally, correlated) states[3,4,10]. Inhomogeneity is thought to arise in some of these systems because of phase separation; however, it can also be tunably engineered, for example, in hybrid superconductor–normal–superconductor (SNS) systems, such as the arrays studied here. In arrays of SNS junctions, the diffusion of electron pairs from the superconductor into the normal metal[11–13]—known as the proximity effect—gives rise to global superconductivity, through a transition typically described using the phenomenological theory of Lobb, Abraham and Tinkham (LAT)[14]. According to the LAT theory, the $T = 0$ state is always superconducting, and no zero-temperature metallic state should appear.

Most previous studies of SNS arrays used islands much larger than the superconducting coherence length $\xi_{SC}$ (that is, having well-defined superconductivity)[1]; however, there is evidence that arrays of mesoscopic islands (that is, islands of dimensions comparable to $\xi_{SC}$) exhibit behaviour that deviates from the LAT theory[5,15], and might therefore possess non-superconducting $T = 0$ states. Furthermore, the dependence of the superconducting transition on key parameters—such as island spacing and size—has not previously been studied systematically. In this Letter, we present transport measurements on arrays of mesoscopic niobium (Nb) islands having systematically varying inter-island spacings, placed on patterned gold (Au) films. We observe that the device resistance drops to zero in two steps as the temperature is lowered. The lower-temperature drop, at temperature $T_2$, is associated with superconducting phase-locking across the array; the data show that the dependence of $T_2$ on island spacing and thickness deviates strongly from LAT theory. Surprisingly, the higher-temperature drop, at $T_1$, traditionally associated with the superconducting transition of each island, also depends strongly on the island spacing, and seems to extrapolate to zero at finite spacings. This observation implies that superconductivity on individual islands is fragile, and that a $T = 0$ metallic state might be realizable for very weakly coupled islands.

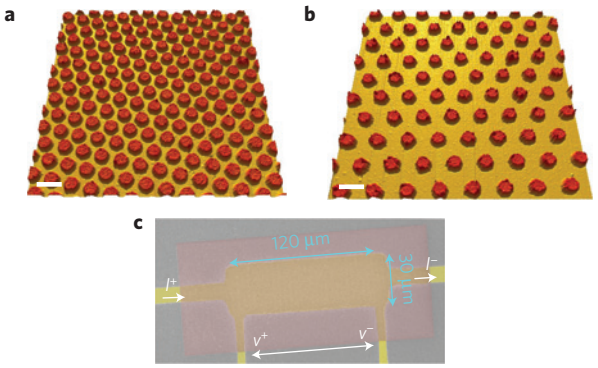


**Figure 1 | AFM topography of arrays of Nb islands on Au and SEM image of device. a**,**b**, AFM images of arrays of 87-nm-thick Nb islands (red) on 10-nm-thick Au underlayer (yellow). Each array has an edge-to-edge spacing of 140 nm (**a**) and 340 nm (**b**). The scale bar is 500 nm. **c**, False colour SEM image of island array (red rectangle) overlapping Au four-probe pattern (yellow), with the measurement schematic indicated.

Our samples consist of 10 nm-thick Au, patterned for four-point transport measurements, on $Si/SiO_2$ substrates (see Methods for fabrication details). The Au patterns are overlaid with triangular arrays of 260 nm diameter Nb islands, as shown in Fig. 1. Each array contains more than 10,000 Nb islands. The data in this Letter are from two sets of devices: having 87-nm (±2 nm)- and 145-nm (±2 nm)-thick Nb islands respectively. The devices in each set are identical, except for varied island spacing. X-ray diffraction and scanning electron microscopy of the Nb revealed columnar grains ~30 nm in diameter, typical of evaporated Nb (ref. 16); thus,

[1]Department of Physics and Frederick Seitz Materials Research Laboratory, 104 South Goodwin Avenue, The University of Illinois Urbana-Champaign, Urbana, Illinois 61801-2902, USA, [2]School of Physics, Georgia Institute of Technology, 837 State Street, Atlanta, Georgia 30332-0430, USA.
*e-mail: nadya@illinois.edu.

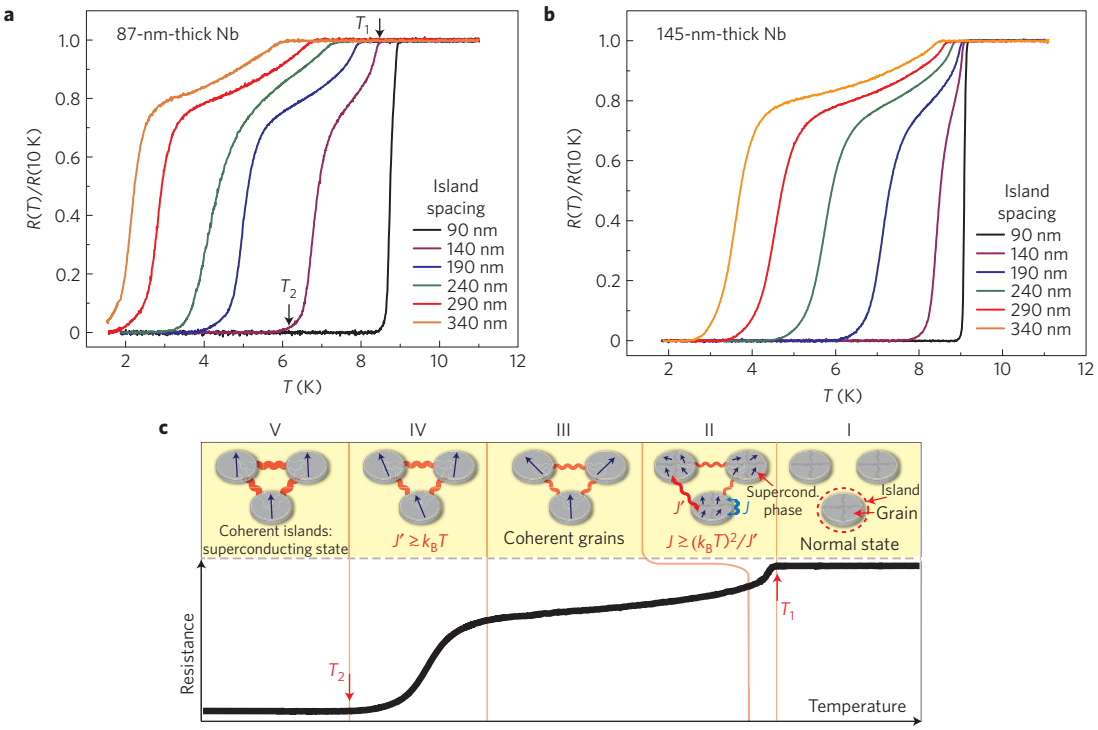


**Figure 2 | Superconductivity in Nb island arrays. a**,**b**, Temperature dependent resistive transitions in arrays having different edge-to-edge island spacings. The island diameter is 260 nm for all arrays. The islands are 87 nm thick (**a**) and 145 nm thick (**b**). Black arrows in **a** mark $T_1$ and $T_2$ for the islands spaced 140 nm apart. The data are normalized to the resistance at 10 K. Note that $T_1$ and $T_2$ occur at higher temperatures for thicker islands. In **a**, the lowest temperature curves are cut off by the minimum attainable temperature of our apparatus. **c**, The curve illustrates two-step resistance versus temperature behaviour, with the island transition marked at $T_1$, and film transition marked at $T_2$. Pictures show three islands, each limited to four grains for simplicity. In region I, the Nb islands are normal metals. In region II, the phase of the grains (represented by arrows) starts to become coherent throughout each island (although there is not yet inter-island phase coherence). At $T_1$, Cooper pairs diffuse from the Nb into the Au, and the resistance drops. The grains have intra-island Josephson coupling $J$ and nearest-neighbour inter-island coupling $J'$(represented by red squiggly lines). In region III, $J$ has saturated, but $J'$ continues to increase as the normal metal coherence length $\xi_N$ increases. In region IV, $\xi_N$ becomes comparable to the island spacing, and the entire system of film and islands progresses towards having global phase coherence. As the temperature is further decreased, the film undergoes a transition to a superconducting state at $T_2$.

each Nb island contains ~50–100 grains. The superconducting coherence length of Nb is estimated to be ~27 nm (see Methods), comparable to the grain size but smaller than the island size.

Figure 2 shows resistance measurements for the devices, as well as an illustration of the two-step development of superconductivity. The data in Fig. 2a,b show that both $T_1$ and $T_2$ decrease with increasing island spacing. The resistance exhibits an abrupt change in slope at $T_1$, but not the sharp drop seen for larger islands[1]. Figure 3 shows a plot of $T_1$ versus island spacing. It is evident that $T_1$ decreases more rapidly for the shorter islands, but seems to decrease linearly with spacing for both the shorter and taller islands, extrapolating to zero at ~840 nm and ~2,600 nm, respectively. The resulting $T = 0$ states would thus be metallic in that they would have finite resistance at finite island spacing. The data in Fig. 2 also show that $T_2$ is more strongly depressed for shorter islands than for taller islands. As schematized in Fig. 2c, these trends can be understood using a model of coupled islands, each composed of grains, having two characteristic energy scales: (1) $J$, the coupling between grains on an individual island, and (2) $J'$ ($<J$), the coupling between grains on neighbouring islands. According to this scheme, for $T > T_1$, the separate grains on each island have incoherent superconducting phases; at $T_1$, intra-island phase coherence develops, and the system's resistance decreases. For very large islands, $T_1$ would depend only on $J$, which grows with island height but is spacing-independent. For mesoscopic islands, however, the $T_1$ of an isolated island is depressed (possibly to $T = 0$) by phase fluctuations among the grains; the inter-island coupling $J'$ serves to reduce these fluctuations by increasing the effective 'dimensionality' of the island system, thereby stabilizing superconductivity. Thus, $T_1$ decreases for larger spacings (that is, as $J'$ decreases). Below $T_1$, the intra-island phase coherence strengthens continuously (Fig. 2c, region II); thus, the system resistance continuously decreases rather than steeply dropping at $T_1$. Region III of Fig. 2c shows the familiar proximity behaviour; here, the normal-metal coherence length[17] $\xi_N$ increases until it becomes comparable to the island spacing. Then, inter-island phase coherence begins to emerge (Fig. 2c, region IV), and at $T_2$ the system undergoes a Berezinskii–Kosterlitz–Thouless transition to a fully superconducting state[1,2].

The inset to Fig. 4 shows how $T_2$ decreases with increasing island spacing. For each device, $T_2$ was extracted by measuring the temperature at which current–voltage ($I$–$V$) curves became nonlinear (see Supplementary Information). The dependence of $T_2$ on array parameters deviates from LAT theory both quantitatively (that is, $T_2$ decreases more rapidly with island spacing than predicted) and qualitatively (that is, $T_2$ depends strongly on island height). Figure 4 also shows the systematic dependence of $\xi_N(T_2)$ on island spacing, where $\xi_N = \sqrt{\hbar D/(k_B T)}$ and the normal-metal diffusion constant $D \approx 94\ \mathrm{cm^2\ s^{-1}}$ (see Methods). We observe $\xi_N(T_2)$ to vary approximately linearly with island spacing.

We now turn to a more quantitative description of these transitions. From the Ginzburg–Landau perspective, $T_1$ for an isolated island of lateral dimensions comparable to $\xi_{SC}$ should equal the transition temperature for a continuous film of the same height, because the suppression of superconductivity due to

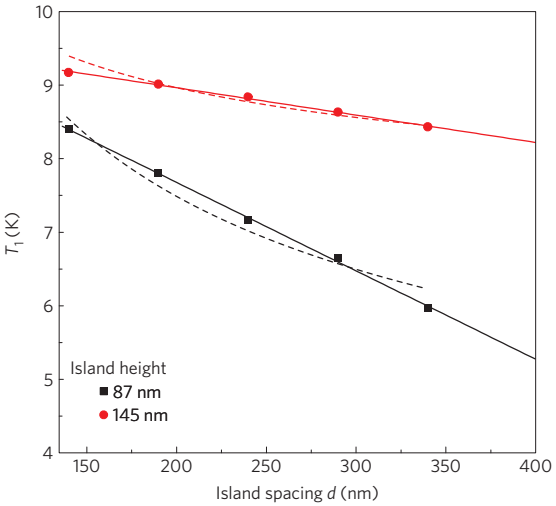


**Figure 3 | Dependence of $T_1$ on array geometry.** The first transition temperature $T_1$ is plotted versus island spacing for 87-nm-thick islands (black squares) and 145 nm thick islands (red circles). Solid lines are linear fits and dashed curves are fits to equation (3), that is, the coupled-XY-chain model, in which the coupling $J_0$ and the length scale $\alpha$ are treated as fit parameters (see text and Methods). $J_0$ depends strongly on island height, but $\alpha$ is approximately constant. The points for the smallest island spacings are not shown, as the transitions for this spacing do not show two steps; for a similar reason, the 140 nm spacing for the thicker islands is shown, but not included in the fit.

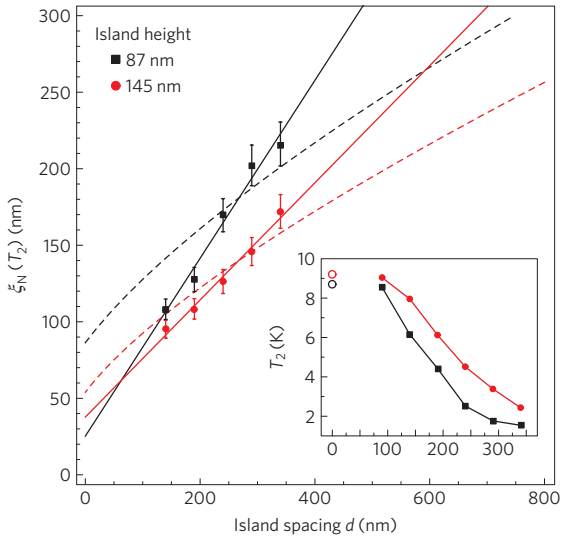


**Figure 4 | Dependence of $T_2$ on array geometry.** The normal-metal coherence length at $T_2$, $\xi_N(T_2)$, is shown as a function of island spacing. The temperature $T_2$ for each device was extracted from the temperature-dependence of $I$–$V$ curves (see Supplementary Information). The error bars primarily result from uncertainty in the diffusion constant (due to the standard deviation in the Au resistance at 10 K). Solid lines are linear fits and dashed lines are fits to LAT theory (ref. 14). The point for the closest spaced islands is excluded from the plot, as for them the transition shows only one step. The inset shows $T_2$ for each device versus edge-to-edge spacing, for 87-nm-thick islands (black squares) and 145-nm-thick islands (red circle). The open circles mark the $T_c$ of the unpatterned bilayers (8.75 K and 9.1 K, respectively).

superconductor–vacuum interfaces at the sides is negligible[13,18]. This expectation is inconsistent with the pronounced spacing-dependence seen in the data. Because the islands are themselves granular, we attribute the unexpected depression of $T_1$ to spatial fluctuations of the superconducting phase within each island, that is, among the constituent grains, which have lateral dimensions comparable to $\xi_{SC}$. The basic physics of the trend of $T_1$ can be captured by a simple XY model[19], governed by the Hamiltonian:

$$H = -J\sum_{p}\sum_{\langle ij\rangle\in p}\cos(\theta_i-\theta_j) - J'\sum_{\langle pp'\rangle}\left(\sum_{i\in p}\cos(\theta_i)\right)\left(\sum_{j\in p'}\cos(\theta_j)\right) \quad (1)$$

where $\theta_i$ is the superconducting phase of grain $i$, $p$ indexes islands, $\langle ij\rangle \in p$ denotes nearest-neighbour grains on island $p$, and $\langle pp'\rangle$ denotes nearest-neighbour islands. Each grain on an island is assumed to couple with equal strength to every grain on neighbouring islands; hence the inter-island interaction $J'$ can be regarded as 'mean-field'. The temperature dependence of $J'$ is taken to have the standard proximity form[2,14]: $J'(T) \approx J'_0\exp(-d/\xi_N(T))$, where $d$ is the edge-to-edge spacing of the islands and $J'_0$ is the coupling amplitude. To reproduce the strong depression of $T_1$ for widely spaced islands, we approximate each island as a one-dimensional chain of XY spins.

Although one-dimensional coupled spins are by no means a fully realistic description of the experimental system, this model captures the following key features of the data: (1) the strong, non-saturating depression of $T_1$, and (2) the two-step character of the transition, that is, the fact that $T_1 > T_2$ so that intra-island ordering occurs before inter-island ordering (see Methods for details). Fits to the XY-chain model are shown in Fig. 3, and agree reasonably well with the experimental data. The most notable discrepancy involves the largest (340 nm) spacing for the thinner islands, for which $T_1$ is lower than the model predicts; this might suggest that other —possibly quantum—fluctuations are significant in this regime.

We now turn to the spacing- and height-dependence of $T_2$. As seen in Fig. 4, $\xi_N(T_2)$ depends approximately linearly on $d$; such a relationship implies, in particular, that for large $d$ the transition occurs when $d/\xi_N(T_2)$ is a constant. This observation conflicts with the LAT theory[2,14] (presumed to be valid for our measurement regime of $d > \xi_N$), which predicts that $k_B T_2 \sim J'_0\exp[-d/\xi_N(T_2)]$ (see fits in Fig. 4). The asymptotic constancy of $d/\xi_N(T_2)$ can be accounted for in one of two ways. The first is to modify the LAT theory by replacing the proximity expression for $J'$ with the quasiclassical $T = 0$ expression[12], $J' \sim 1/d^2$. This replacement, strictly valid only for $d \leq \xi_N(T_2)$, would yield a modified LAT threshold of the form $T_2 \sim 1/d^2$, and consequently a linear relationship between $d$ and $\xi_N(T_2)$. Although this modification of LAT theory reproduces the observed linear relationship, it cannot explain the height-dependence of $T_2$. An alternative explanation, which captures both the linear relationship and the height-dependence, is to retain the proximity-effect form of $J'$ but assume the existence of a mesoscopic energy scale on each island (an effective 'charging energy' or, alternatively, the electronic level spacing on a grain (M.V. Feigel'man, personal communication)) that competes with superconductivity. In this scenario $T_2$ would occur when $J'_0\exp[-d/\xi_N(T_2)] = \kappa$ for some constant $\kappa$; this implies the existence of a minimum inter-island coupling $\kappa$ that must be overcome for superconductivity to be attained, even at $T = 0$, and consequently the possibility of a $T = 0$ metallic state.

Both phase transitions studied in this work occur at temperatures that seem to extrapolate to zero, suggesting the existence of two quantum phase transitions; in particular, our devices may approach a quantum superconductor–metal transition, which has been predicted but not observed[3–5,10]. The tunability of our devices—including the ability to vary island geometry, spacing, material

properties and disorder—thus makes them excellent test-beds for exploring such transitions. The unconventional metallic state we observe at temperatures between $T_1$ and $T_2$ is similar to that predicted for phase-separated quantum metals[4,5] in that it possesses 'regional' phase correlations, that is, correlations at length-scales larger than that of single islands but not global in extent. The ability to stabilize regional correlations, in the absence of long-range ordering, is characteristic of a variety of inhomogeneous correlated systems, including high-temperature superconductors[20], coupled magnetic chains[21], and strained superconducting films[22]. The tunability of our system could thus help elucidate open questions in these materials.

## Methods

**Samples.** Standard photolithographic techniques and electron beam evaporation were used to create the 10-nm-thick four-point pattern of Au with a 4 Å Ti adhesion layer. The Nb islands were then patterned using electron-beam lithography. Before electron beam evaporation of the Nb islands (in an ultrahigh vacuum system at $\sim 10^{-9}$ torr), the Au surface was $Ar^+$ ion milled to establish a clean interface. For each sample, six arrays were patterned onto a single $Si/SiO_2$ substrate, each with different edge-to-edge spacings: $d = 90$ nm, 140 nm, 190 nm, 240 nm, 290 nm and 340 nm. Four other samples were fabricated; all showed similar data trends, but had limited data ranges (for example, fewer working devices).

The measurement area of every device is $120\,\mu m \times 30\,\mu m$, so the number of islands in each array ranges from 11,400 to 33,516, depending on the island spacing. The large number of islands ensures that discrete percolation paths or individual junction properties do not dominate the conductance. All Nb islands are 260 nm in diameter, which is about 10 times the Nb Ginzburg–Landau dirty-limit coherence length $\xi_{SC}^{Nb}(T_c \approx 9.1\,K) \approx 27$ nm, for an approximate mean free path $l \approx 8$ nm. We estimate $l$ from the Einstein relation, using the normal state resistivity $\rho(10\,K) \approx 1.12 \times 10^{-5}\,\Omega$ cm near the transition of an 87-nm-thick unpatterned Nb film. X-ray diffraction spectra of Nb films and scanning electron microscopy of Nb islands showed that the Nb is polycrystalline with growth along the (110) direction, and grain height equivalent to the film thickness. Scanning electron microscope (SEM) images revealed an elongated, columnar grain structure. The Au film resistivity in all devices is $\rho(10\,K) \approx (6.25 \pm 0.75) \times 10^{-6}\,\Omega$ cm, which is extracted from unpatterned 10-nm-thick films. Using the Einstein relation, we estimate a diffusion constant $D \approx 94.2\ cm^2\ s^{-1}$, which yields a mean free path of $l \approx 13$ nm and a temperature-dependent coherence length $\xi_N(T) \approx 268/\sqrt{T}$ nm.

**Measurement.** All measurements above 1.5 K were carried out in a pumped He-4 cryostat, whereas lower temperature measurements were performed in a He-3 refrigerator. Resistance was measured by standard, low-frequency a.c. lock-in techniques using an excitation current of 500 nA. To minimize Joule heating, $I$–$V$ characteristics were measured using rectangular current pulses, with a current-on time of 3.5 ms and current-off time of 3 ms.

**Coupled-chain model.** The model of coupled XY spin chains introduced in the main text can be shown to have the following properties: (a) strong, non-saturating depression of $T_1$ for widely spaced islands, and (b) a value of $T_1$ that is nevertheless greater than the inter-island coherence temperature $T_2$. By exploiting a mapping between the XY chain and a quantum mechanical rotor[23], one can show that the threshold for an island to acquire a well-defined superconducting phase in the mean field of neighbouring islands is

$$\frac{k_B T_1}{\sqrt{zJJ'}} \coth\left(m\sqrt{\frac{zJ'}{J}}\right) \approx 1 \qquad (2)$$

where $z$ is the coordination number of each island (six for a triangular array) and $m$ is the number of grains on each island. This model satisfies property (a) because equation (2) allows for $T_1 = 0$ at $J' = 0$ (that is, isolated islands are not superconducting). The model also satisfies property (b) as follows. For temperatures well below $T_1$, the phases of the grains on an individual island are mutually locked; hence, one can neglect the first term of equation (1). Then, $T_2$ is given by $zmJ'(T_2) \approx k_B T_2$. Comparing expressions for $T_1$ and $T_2$, we find two separate transitions (that is, $T_2 < T_1$) provided that $m < \sqrt{J/J'}$; this condition always holds for large $J$. If we take $J$ to have the proximity-effect form $J \approx J_0 \exp(-\alpha/\xi_N)$, with $\alpha$ being a constant that is weakly dependent on individual-island parameters, then equation (2) can be rearranged to yield the following dependence of $\xi_N$ on $d$:

$$d + \alpha = -\ln\left[J_0 J_0'/\xi_N^2(T_1)\right]\xi_N(T_1) \qquad (3)$$

Figure 3 shows that fits of the data to equation (3) are reasonable. Note that the lack of saturation of $T_1$ seen in the data and reproduced by the model is consistent with a value of $T_1 = 0$; this admits the possibility of a $T = 0$ metallic state, similar to that described in ref. 4.

Received 13 July 2011; accepted 26 October 2011; published online 4 December 2011

## References


1. Resnick, D. J., Garland, J. C., Boyd, J. T., Shoemaker, S. & Newrock, R. S. Kosterlitz–Thouless transition in proximity-coupled superconducting arrays. *Phys. Rev. Lett.* **47,** 1542–1545 (1981).
2. Abraham, D. W., Lobb, C. J., Tinkham, M. & Klapwijk, T. M. Resistive transition in two-dimensional arrays of superconducting weak links. *Phys. Rev. B* **26,** 5268–5271 (1982).
3. Feigel'man, M. V., Larkin, A. I. & Skvortsov, M. A. Quantum superconductor–metal transition in a proximity array. *Phys. Rev. Lett.* **86,** 1869–1872 (2001).
4. Spivak, B., Zyuzin, A. & Hruska, M. Quantum superconductor-metal transition. *Phys. Rev. B* **64,** 132502 (2001).
5. Spivak, B., Oreto, P. & Kivelson, S. A. Theory of quantum metal to superconductor transitions in highly conducting systems. *Phys. Rev. B* **77,** 214523 (2008).
6. Abrahams, E., Kravchenko, S. V. & Sarachik, M. P. Metallic behavior and related phenomena in two dimensions. *Rev. Mod. Phys.* **73,** 251–266 (2001).
7. Kapitulnik, A., Mason, N., Kivelson, S. A. & Chakravarty, S. Effects of dissipation on quantum phase transitions. *Phys. Rev. B* **63,** 125322 (2001).
8. Abrahams, E., Anderson, P. W., Licciardello, D. C. & Ramakrishnan, T. V. Scaling theory of localization: Absence of quantum diffusion in two dimensions. *Phys. Rev. Lett.* **42,** 673–676 (1979).
9. Phillips, P. & Dalidovich, D. The elusive Bose metal. *Science* **302,** 243–247 (2003).
10. Phillips, P., Wan, Y., Martin, I., Knysh, S. & Dalidovich, D. Superconductivity in a two-dimensional electron gas. *Nature* **395,** 253–257 (1998).
11. Gueron, S., Pothier, H., Birge, N. O., Esteve, D. & Devoret, M. H. Superconducting proximity effect probed on a mesoscopic length scale. *Phys. Rev. Lett.* **77,** 3025–3028 (1996).
12. Dubos, P. *et al.* Josephson critical current in a long mesoscopic S–N–S junction. *Phys. Rev. B* **63,** 064502 (2001).
13. De Gennes, P. G. Boundary effects in superconductors. *Rev. Mod. Phys.* **36,** 225–237 (1964).
14. Lobb, C. J., Abraham, D. W. & Tinkham, M. Theoretical interpretation of resistive transition data from arrays of superconducting weak links. *Phys. Rev. B* **27,** 150–157 (1983).
15. Kouh, T. & Valles, J. M. Deviations from mean-field behavior in disordered nanoscale superconductor–normal-metal–superconductor arrays. *Phys. Rev. B* **67,** 140506 (2003).
16. Asada, Y. & Nose, H. Superconductivity of niobium films. *J. Phys. Soc. Jpn* **26,** 347–354 (1969).
17. Imry, Y. *Introduction to Mesoscopic Physics* (Oxford Univ. Press, 1997).
18. Werthamer, N. R. Theory of the superconducting transition temperature and energy gap function of superposed metal films. *Phys. Rev.* **132,** 2440–2445 (1963).
19. Chaikin, P. M. & Lubensky, T. C. *Principles of Condensed Matter Physics* (Cambridge Univ. Press, 1995).
20. Kivelson, S. A. *et al.* How to detect fluctuating stripes in the high-temperature superconductors. *Rev. Mod. Phys.* **75,** 1201–1241 (2003).
21. Yasuda, C. *et al.* Neel temperature of quasi-low-dimensional Heisenberg antiferromagnets. *Phys. Rev. Lett.* **94,** 217201 (2005).
22. Glatz, A., Aranson, I. S., Baturina, T. I., Chtchelkatchev, N. M. & Vinokur, V. M. Self-organized superconducting textures in thin films. *Phys. Rev. B* **84,** 024508 (2011).
23. Sachdev, S. *Quantum Phase Transitions* (Cambridge Univ. Press, 1999).


## Acknowledgements

This research was supported by the US Department of Energy (DOE)-Division of Materials Science (DMS) under grant DE-FG02-07ER46453 through the Frederick Seitz Materials Research Laboratory at the University of Illinois at Urbana-Champaign, and partly carried out in the Materials Research Laboratory Central Facilities (partially supported by the DOE under DE-FG02-07ER46453 and DE-FG02-07ER46471). P.M.G. acknowledges partial support of National Science Foundation grant DMR09-06780.

## Author contributions

N.M. conceived and designed the experiments. S.E. carried out the experimental work. S.G. and P.M.G. carried out the theoretical analysis. All authors analysed the results and commented on the manuscript.

## Additional information

The authors declare no competing financial interests. Supplementary information accompanies this paper on www.nature.com/naturephysics. Reprints and permissions information is available online at http://www.nature.com/reprints. Correspondence and requests for materials should be addressed to N.M.